Psychoacoustic Evaluation of an Optimized Low-Noise Drone Propeller Design

Merino Martinez, R.; Ben-Gida, H.; Snellen, M.

Publication date
2024

Document Version
Final published version

Published in
Proceedings of the 30th International Congress on Sound and Vibration

Citation (APA)
Merino Martinez, R., Ben-Gida, H., & Snellen, M. (2024). Psychoacoustic Evaluation of an Optimized Low-Noise Drone Propeller Design. In W. van Keulen, & J. Kok (Eds.), *Proceedings of the 30th International Congress on Sound and Vibration* Article 365 (Proceedings of the International Congress on Sound and Vibration). Society of Acoustics.
https://iiav.org/content/archives_icsv_last/2024_icsv30/content/papers/papers/full_paper_365_20240331054028380.pdf

PSYCHOACOUSTIC EVALUATION OF AN OPTIMIZED LOW-NOISE DRONE PROPELLER DESIGN

Roberto Merino-Martínez, Hadar Ben-Gida, and Mirjam Snellen

Aircraft Noise and Climate Effects, Delft University of Technology, Delft, The Netherlands

E-mail: r.merinomartinez@tudelft.nl

The noise emissions of an optimized low-noise drone propeller design were measured experimentally using a polar array consisting of fifteen microphones within a circular arc covering 105 degrees. The experiments were conducted in the anechoic chamber at the Faculty of Aerospace Engineering at the Technion - Israel Institute of Technology. A comparison between the optimized low-noise drone propeller design and the baseline case (a commercial off-the-shelf APC $14'' \times 5.5''$ propeller) was performed using conventional sound metrics (e.g. equivalent A-weighted sound pressure level or perceived noise level), as well as state-of-the-art psychoacoustic sound quality metrics (loudness, sharpness, tonality, roughness, and fluctuation strength). These sound quality metrics (SQMs) were also combined into a global psychoacoustic annoyance metric to assess the predicted noise annoyance a human observer would experience. Despite increasing noise levels at the lower frequencies, the optimized configuration presents consistently lower noise emissions in the directivity angles considered for all the sound metrics employed. These results encourage further research into the perception-influenced design of drone propellers by focusing on psychoacoustic metrics that capture human hearing more accurately than conventional sound metrics typically used in certification.

Keywords: drone noise, propeller noise, psychoacoustics, sound quality metrics, aeroacoustics

1. Introduction

The relatively low cost and simple usage of small unmanned aircraft systems (sUAS) enabled them to become a growing market within general aviation during the past decade. However, although much technological improvement has been achieved regarding sUAS performance, the noise emissions associated with the operation of such systems remain a challenge. In particular, since most sUAS utilize rotary wing propulsion systems with electric motors, the propeller/rotor is often recognized as the most significant noise source. The propeller noise contains rich tonal and broadband contents due to the periodic rotatory motions of the blades and the surrounding complex turbulent flows, which can adversely impact human health; e.g., broadband noise affects the human auditory evoked response [1] and the tonal noise contributes to annoyance as the human ear is sensitive to the pitch characteristics [2]. As a result, there has been a growing interest in propeller noise reduction strategies in recent years [3].

The use of conventional sound metrics for noise annoyance assessment (e.g., equivalent A-weighted sound pressure level $L_{\mathrm{p,A,eq}}$) is questionable because they fail to capture important sound characteristics that cause annoyance [4, 5]. Therefore, the current study also employs psychoacoustic sound quality metrics (SQMs) [6] to assess the perception of the noise emissions of two different drone propeller designs.

The manuscript is organized as follows: Section 2 explains the design process for the optimized drone propeller, the experimental setup, and the sound metrics considered in this study. The results obtained are discussed in section 3, whereas section 4 presents the main conclusions.

2. Methodology

2.1 Propeller design process

Two propellers were studied herein: a baseline and an optimized propeller. The baseline propeller considered corresponds to the commercial off-the-shelf APC $14'' \times 5.5''$ propeller [1], made of nylon; this propeller has a diameter of $D_{\text{prop}} = 14'' = 355.6\,\text{mm}$ and a pitch of $5.5''$. The optimized low-noise signature propeller was derived from a perception-influenced optimization design process using the getPROP suite [7]. The getPROP framework enables an end-to-end analysis, from an initial propeller design to a low-noise signature optimized configuration that meets the desired operational requirements. The code consists of various modules, such as aerodynamic modeling, performance computation, aeroacoustic prediction, atmospheric attenuation, psychoacoustics, and multi-objective optimization.

The psychoacoustic module in the getPROP code involves computing the attenuated acoustic spectrum (under specific background noise) in critical bands, following Zwicker's formalism [4]. Then, the loudness metric N is computed as a function of the observer's distance s and azimuth angle θ from the propeller's axis (see Fig. 1). A signal is assumed not noticeable by a human ear when the loudness value is $N \leq 0.1$ sone. The detection range R_d is calculated (from (θ, s)) based on the minimum horizontal distance s between the propeller and the observer for which $N \leq 0.1$ sone; i.e., the detection range is a threshold range from which the observer notices the propeller at first.

In the getPROP analysis, the propeller disk radius ($R_{\text{prop}} = 177.8\,\text{mm}$) and the number of blades ($B = 2$) were preserved to allow a reasonable comparison to the reference propeller. The blade sections of the baseline propeller consist of a NACA5608 airfoil shape, whereas a low-Reynolds FX63-137 airfoil was selected for the optimized propeller design to improve its performance in the low-Reynolds number regime [8]. The design thrust point for both propellers is $T_{\text{DP}} = 9.5\,\text{N}$.

The optimized propeller was derived from a multi-objective optimization process (using a genetic algorithm) set to yield a propeller design with a minimum detection range, R_d, and minimal required power at the design point, P_{DP}. The geometrical variables changing throughout the optimization process were the blade's radial chord distribution $c(r)$ and the pitch angle distribution $\beta(r)$, see Fig. 1a. Three constraints are set to prevent diverging from the reference design's performance. The first one corresponds to the blade's aspect ratio, $AR = R_{\text{prop}}^2/S_{\text{ref}} \geq 6$, where S_{ref} is the surface area of a single propeller blade. The second one is related to the propeller's figure-of-merit, $FM = \sqrt{2}C_T^{1.5}/(4\pi C_Q) \geq 0.68$, where C_T and C_Q are the thrust and torque coefficients, respectively. A third constraint sets the maximum motor shaft torque required for the optimal propeller design at maximum thrust. Otherwise, the propeller might not be able to achieve the maximum required thrust for a given system using an existing motor. The optimization process resulted in a Pareto front with multiple propeller designs, from which a desired optimized low-noise signature propeller design was selected. The radial distributions of the blade's chord normalized by the propeller radius $c(r)/R_{\text{prop}}$ and pitch angle $\beta(r)$ for the baseline and optimal propellers are depicted in Fig. 1a.

The optimal propeller design was manufactured from carbon fiber, with the blades attached to an aluminum hub (with a radius of $R_h = 0.14R_{\text{prop}}$). To satisfy the minimum blade thickness threshold ($2t^* = 0.2\,\text{mm}$) allowed for manufacturing, the trailing-edge region of the optimal propeller design had

[1] APC $14'' \times 5.5''$ propeller website: https://www.apcprop.com/product/14x5-5mr/

to be modified. Therefore, the upper (y_{uc}) and lower (y_{lc}) curves of each blade's section around the mean camber line were modified to satisfy $y_{\mathrm{uc}} - y_{\mathrm{lc}} \geq 2t^*$, with the trailing edge being rounded.

2.2 Experimental setup

2.2.1 Anechoic chamber

Acoustic measurements of both propellers were conducted in the newly-commissioned, fully-anechoic chamber at the Faculty of Aerospace Engineering at the Technion - Israel Institute of Technology. The chamber, designed by Eckel Industries, has physical dimensions of $7\,\mathrm{m} \times 5\,\mathrm{m} \times 5\,\mathrm{m}$ (length $\times$ width $\times$ height), where a metal mesh walking surface extends across most of its projected floor area. The facility has a cut-off frequency of $150\,\mathrm{Hz}$ and a background facility noise level that is below 15 dB (above the cut-off frequency).

2.2.2 Propellers and test rig

The propeller test rig consists of a support structure, a motor coupled with an encoder, and a load cell. The propeller was set up on a cylindrical strut, placed at the center of the anechoic chamber at $0.9\,\mathrm{m}$ ($2.6D_{\text{prop}}$) above the ground. The propeller was powered by a brushless electric motor and controlled using an electronic speed controller. The motor shaft rotational velocity was measured using dedicated optic and electromagnetic encoders placed under the motor hub.

The operation conditions employed for each propeller during the acoustic measurements are presented in Table 1. These conditions were selected because they correspond to the design thrust of $T_{\mathrm{DP}} = 9.5\,\mathrm{N}$ for each propeller. For example, the baseline rotor spun at a rate of $n = 75\,\mathrm{rev/s}$ (i.e., $4,480$ RPM), resulting in a first blade passing frequency of $\mathrm{BPF} = Bn = 149\,\mathrm{Hz}$. The Reynolds number based on the blade chord of $c_{0.75R_{\text{prop}}} = 23\,\mathrm{mm}$ at $r = 0.75R_{\text{prop}}$ is $\mathrm{Re}_{0.75R_{\text{prop}}} = c_{0.75R_{\text{prop}}} 2\pi n 0.75R_{\text{prop}}/\nu = 1.33 \cdot 10^5$, where ν is the kinematic viscosity of air. The tip Mach number is $\mathrm{M_{tip}} = 2\pi n R_{\text{prop}}/a_\infty = 0.245$, where a_∞ is the speed of sound in air, considered as $343\,\mathrm{m/s}$. The optimized propeller design is shown to operate at the design thrust point ($T_{\mathrm{DP}} = 9.5\,\mathrm{N}$) with a considerably lower rotational speed and, hence, lower M_{tip} than the baseline propeller. Reducing these values is commonly known to lower the tonal noise and shift it to the lower frequencies, where the auditory filter responds correspondingly.

Table 1: Operational conditions set for each propeller to yield the design thrust point of $T_{\mathrm{DP}} = 9.5\,\mathrm{N}$.

Propeller	n, rev/s	RPM, rev/min	BPF, Hz	$\mathrm{Re}_{0.75R_{\text{prop}}}$	$\mathrm{M_{tip}}$
Baseline	75	$4,480$	149	$1.00 \cdot 10^5$	0.245
Optimized	61	$3,680$	123	$1.03 \cdot 10^5$	0.201

2.2.3 Acoustic measurements and data processing

The sound pressure in the free field was measured by an arc array consisting of eight G.R.A.S 46AE $1/2''$ free-field microphones and seven B&K Type 4189 $1/2''$ free-field microphones, resulting in a total of fifteen microphones. The microphones were placed symmetrically around the propeller hub at a radial distance of $1.5\,\mathrm{m}$. The circular arc spanned an azimuth angular range of $0^\circ < \theta < 105^\circ$, where $\theta = 0^\circ$, corresponds to the axis of rotation above the propeller's hub, whereas $\theta = 90^\circ$ refers to the rotor disk plane, see the schematic propeller test rig depicted in Fig. 1b. A constant angular increment of $\Delta\theta = 7.5^\circ$ was set between adjacent microphones on the circular arc array. The circular arc array was enfolded by porous absorbing material to mitigate acoustic reflections. Acoustic data were acquired with the sampling frequency of $F_s = 40.225$ kHz for $T_s = 20$ sec. A National Instruments PXIe-4497 system provided the data acquisition, where the encoder and microphone measurements were recorded simultaneously. The interested reader is referred to [7] for further details on the experimental setup.

The acoustic spectra ($\hat{G}_{pp}$) were calculated with Welch's algorithm using a Hanning window. The data was divided into segments of 2^{15} samples with a 50% overlap. This resulted in a frequency resolution of $\Delta f = 1.235$ Hz for the auto-spectral density ($\hat{G}_{pp}$) of the measured signal in Pa^2/Hz. The auto-spectral density is henceforth presented in dB scale as $L_p = 10\log_{10}(\hat{G}_{pp} \cdot \Delta f / p_{\text{ref}}^2)$, where p_{ref} corresponds to the threshold hearing pressure of 20 μPa.

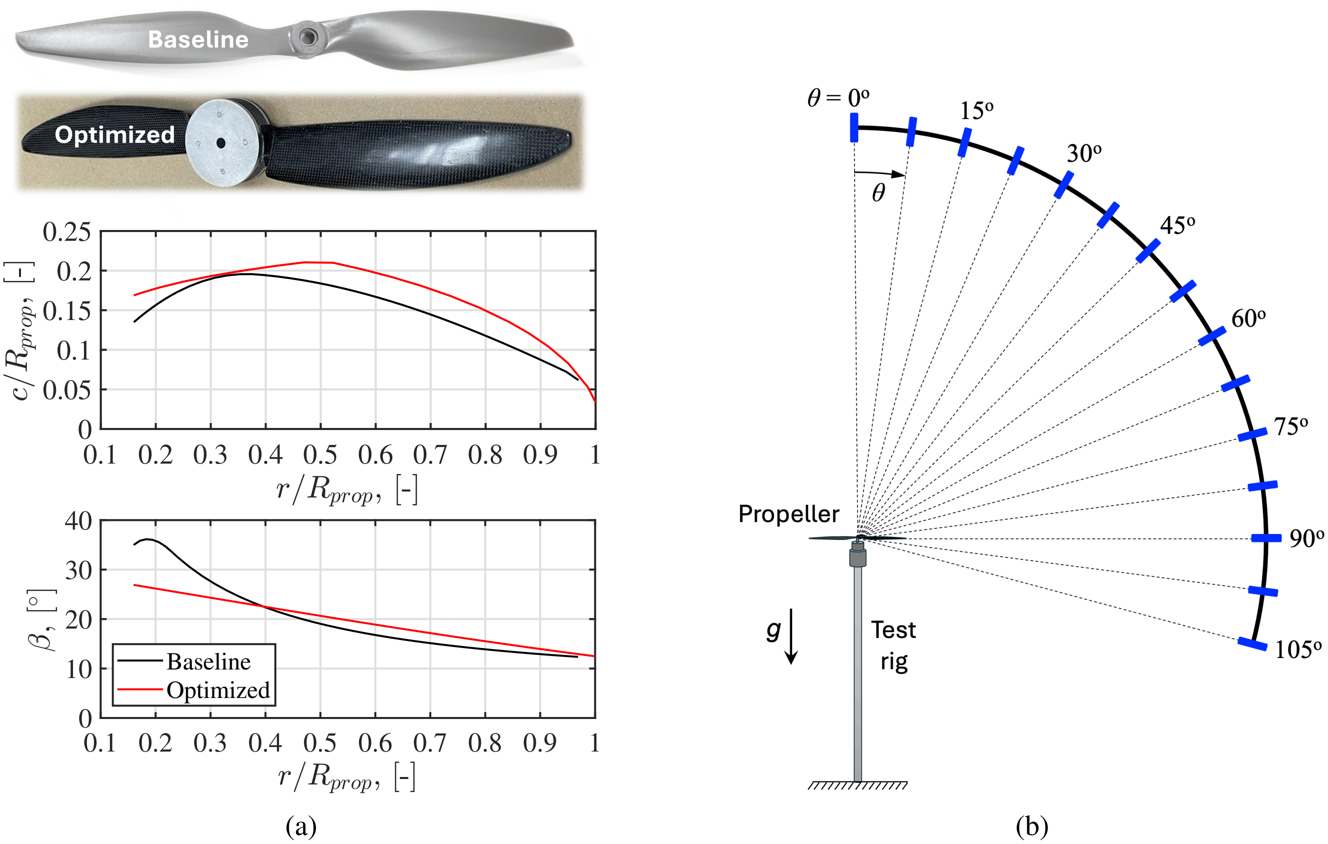

Figure 1: (a) Top: Photographs of both propellers. Center: Radial distribution of the blade's normalized chord (c/R_{prop}), and Bottom: pitch angle (β), for the reference APC $14'' \times 5.5''$ propeller (black) and the optimal design propeller (red) computed by the getPROP software. (b) Schematics of the experimental setup employed, consisting of the propeller test rig and the circular arc array.

2.3 Conventional sound metric evaluation

As mentioned in the introduction, conventional sound metrics typically used in noise assessment pose challenges for quantifying noise annoyance. Nevertheless, current noise regulations still employ these metrics for enforcing environmental noise laws. Therefore, the current study considers the equivalent sound pressure level $L_{\text{p,eq}}$ and its A-weighted version $L_{\text{p,A,eq}}$, as well as the maximum tone-corrected perceived noise level (PNLT) to assess the noise emissions of both propellers. The latter is the base for the effective perceived noise level (EPNL) metric typically employed during aircraft noise certification processes [9].

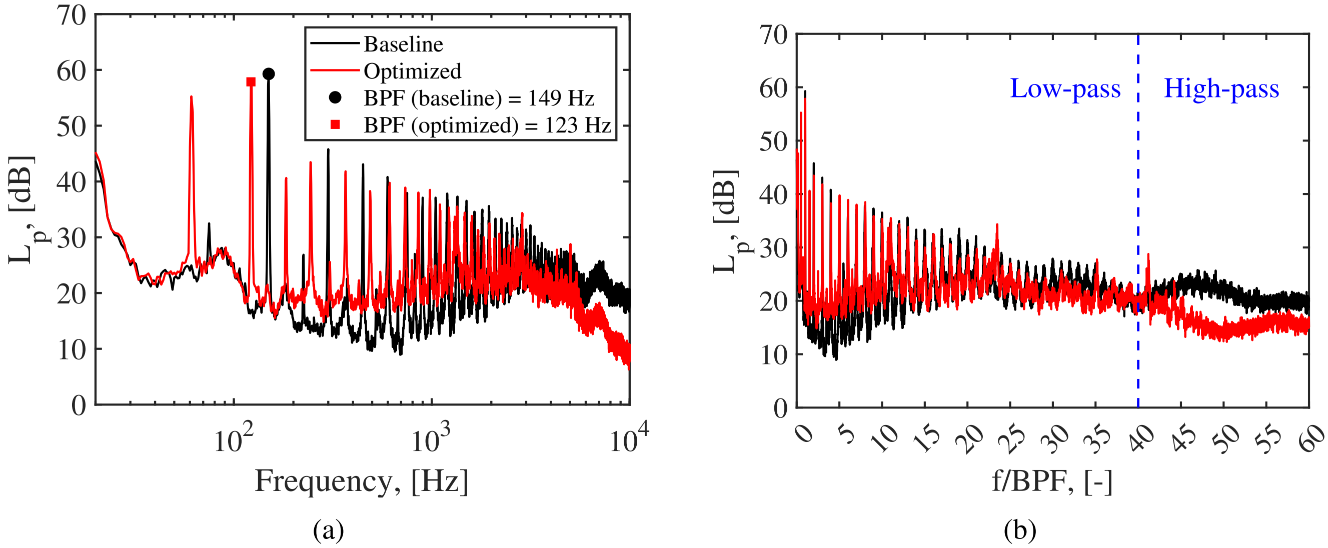

Figure 2: Comparison between the frequency spectra of the baseline and the optimized propellers for an emission angle $\theta = 60°$: (a) Frequency on a logarithmic scale, (b) Linear frequency normalized by the respective BPF.

2.4 Psychoacoustic Sound Quality Metric (SQM) evaluation

Unlike the L_p metric, which quantifies the purely physical magnitude of sound based on the pressure fluctuations, Sound Quality Metrics (SQMs) describe the subjective perception of sound by human hearing. Hence, SQMs are expected to better capture the auditory behavior of the human ear compared to conventional sound metrics typically employed in noise assessments. The five most commonly-used SQMs [6] are:

- Loudness (N): Perception of sound magnitude corresponding to the overall sound intensity.
- Tonality (K): Perceived strength of unmasked tonal energy within a complex sound.
- Sharpness (S): High-frequency sound content.
- Roughness (R): Hearing sensation caused by modulation frequencies between 15 Hz and 300 Hz.
- Fluctuation strength (FS): Assessment of slow fluctuations in loudness with modulation frequencies up to 20 Hz, with maximum sensitivity for modulation frequencies around 4 Hz.

These five SQMs were calculated for each sound wave and combined into a single global psychoacoustic annoyance (PA) metric. Henceforth, the top 5% percentiles of these metrics (values exceeded 5% of the time) are reported (and hence the sub-index *5*). All the SQMs and the PA metric were computed using the open-source MATLAB toolbox SQAT (Sound Quality Analysis Toolbox) v1.1 [10].

3. Results and discussion

3.1 Conventional sound metrics

Figure 2 depicts exemplary frequency spectra for both the baseline and the optimized propellers for an azimuth angle $\theta = 60°$. Figure 2a presents such a comparison by plotting the frequency on a logarithmic scale, showing the different BPF values for the baseline (149 Hz) and optimized (123 Hz) propellers; see Table 1. For a more relevant comparison, Fig. 2b employs a normalized (linear) frequency axis by the respective BPF values in each configuration. As aforementioned in section 2.2, the optimized propeller design presents a lower $\mathrm{M_{tip}}$ value for the design thrust point and, hence, shifts the noise emissions towards lower frequencies ($f < 12\,\mathrm{BPF}$), as depicted in Fig. 2. This is especially the case for the shaft BPF (i.e., half the propeller BPF), which presents values about 22 dB higher for the optimized propeller. This difference is also partly due to the different materials employed for the blades and hub of the optimized propeller. On the other hand, the high-frequency noise emissions ($f > 40\,\mathrm{BPF}$) of the optimized propeller are up to 10 dB lower than for the baseline. Henceforth, the results for certain relevant sound metrics are also reported as low- and high-frequency, after applying, respectively, a low-pass and a high-pass filter with a cut-off frequency of ($f_{\mathrm{cutoff}} > 40\,\mathrm{BPF}$). This cut-off frequency corresponds to 5960 Hz and 4920 Hz for the baseline and optimized propeller, respectively.

The directivity plots of the three conventional sound metrics considered are depicted in Fig. 3. For the $L_{\mathrm{p,eq}}$ metric (Fig. 3a), there are no major differences (below 1.8 dB) between both propellers for all emission angles measured. For the low-frequency noise ($f < 40\,\mathrm{BPF}$), this difference is even smaller (below 0.9 dB). The acoustic radiation patterns of these two cases are also relatively omnidirectional. Despite emitting lower levels, the high-frequency noise ($f \geq 40\,\mathrm{BPF}$) presents considerably lower values for the optimized case (up to 9.5 dB) and a dipole-like radiation pattern typical for propeller noise with minimum emissions around $\theta = 90°$. The $L_{\mathrm{p,A,eq}}$ (Fig. 3b) and $\mathrm{PNLT}_{\mathrm{max}}$ (Fig. 3c) metrics depict the aforementioned dipole-like radiation pattern for all three cases (total, low-frequency, and high-frequency). The major differences between both propellers are also reported for the high-frequency case with values up to 8.8 dBA and 8.2 PNLTdB, respectively. The total and low-frequency noise emissions are comparable between both configurations, with only minor reductions (2.3 dBA and 2.8 PNLTdB) achieved by the optimized propeller.

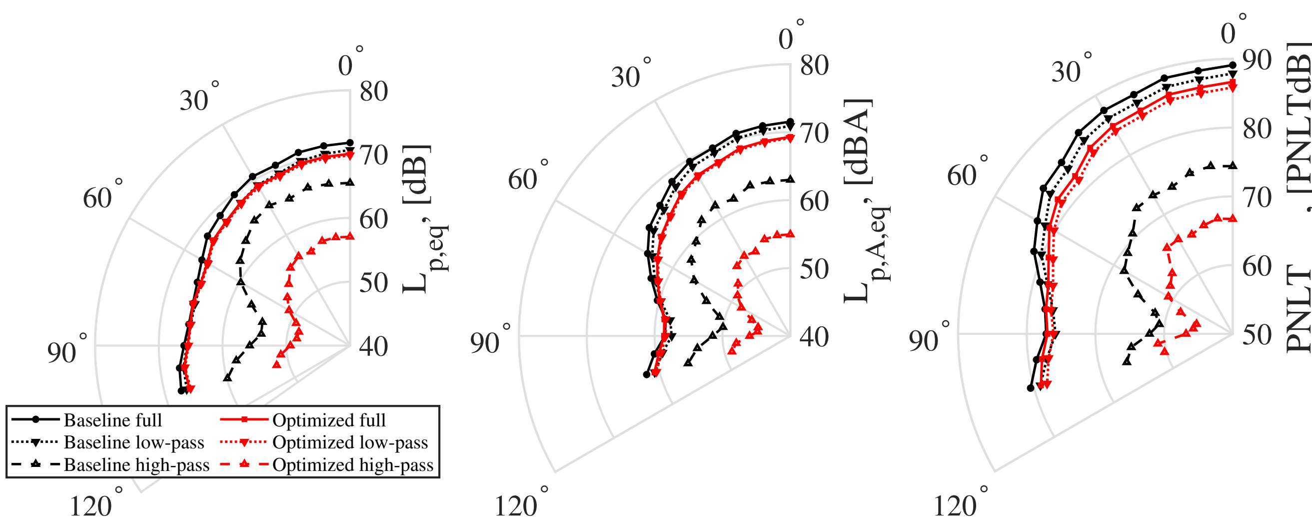

(a) $L_{\mathrm{p,eq}}$ (b) $L_{\mathrm{p,A,eq}}$ (c) Maximum PNLT

Figure 3: Directivity plots for both propellers considering conventional sound metrics and both low-pass and high-pass filters.

3.2 Psychoacoustic sound quality metrics

Figure 4 contains the directivity plots for the five SQMs introduced in section 2.4 and the global PA metric. The loudness metric (N_5, Fig. 4a) depicts comparable radiation patterns as the $L_{\mathrm{p,A,eq}}$ case and reductions up to 3.6 sone offered by the optimized propeller geometry. The tonality (K_5, Fig. 4b) presents considerably high values (up to 0.25 t.u. for the baseline case) and maximum values on the propeller plane ($\theta \approx 90°$). The optimized propeller appears to reduce the tonality to almost half its base-

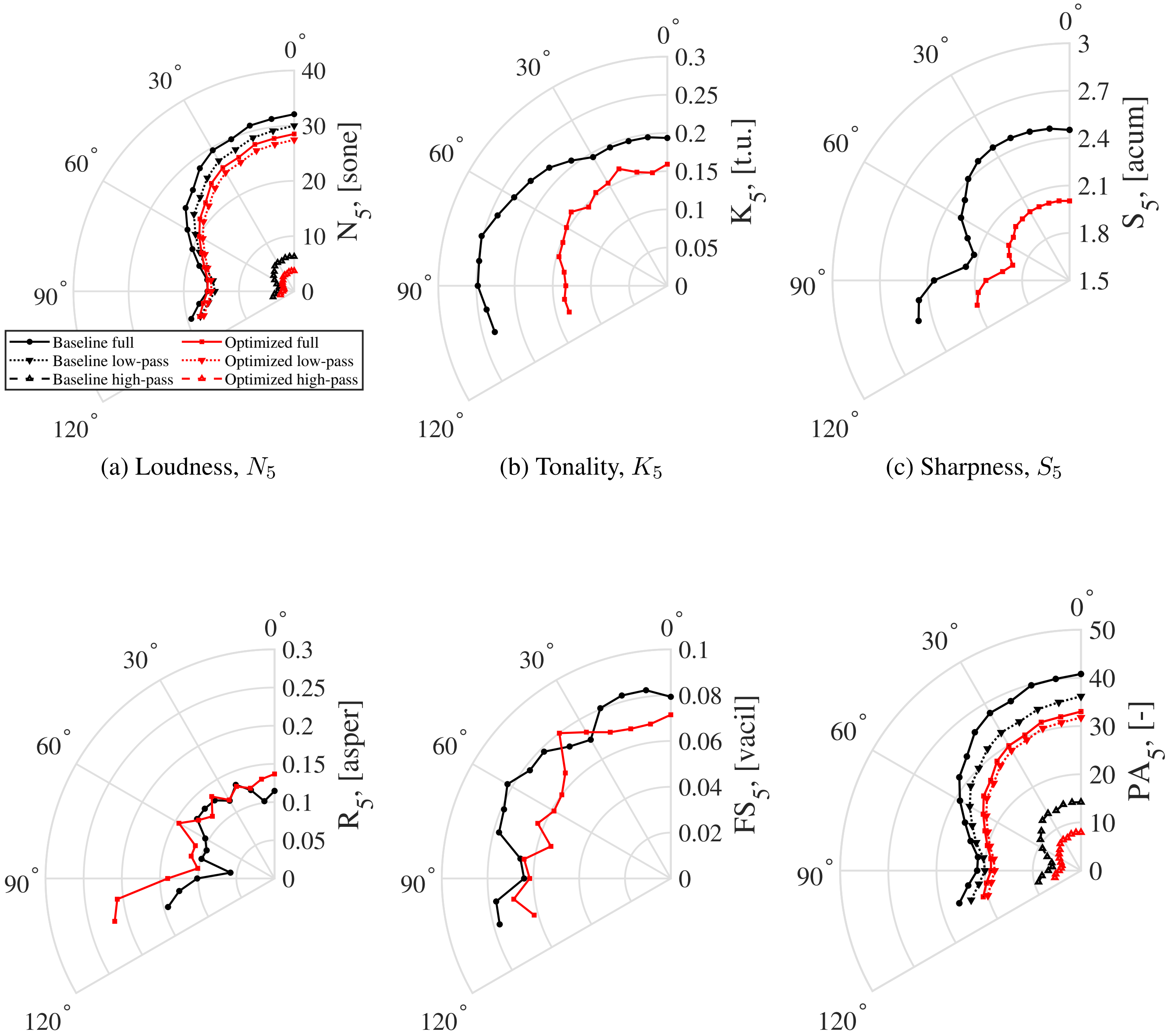

(a) Loudness, N_5 (b) Tonality, K_5 (c) Sharpness, S_5

(d) Roughness, R_5 (e) Fluctuation strength, FS_5 (f) Psychoacoustic Annoyance, PA$_5$

Figure 4: Directivity plots for both propellers considering the top 5% percentiles of the sound quality metrics and (when relevant) both low-pass and high-pass filters.

line value in that direction. This reduction is explained by the generally lower tones observed for this configuration and higher masking by broadband noise, especially at low frequencies, see Fig. 2a. This phenomenon could be due to the expected reduction in leading-edge noise (blade-vortex interaction) for the optimized. As expected from the aforementioned reduction in high-frequency noise, the optimized propeller shows notable reductions in sharpness (S_5, Fig. 4c) up to 0.47 acum. The two metrics related to amplitude modulation (roughness (R_5) and fluctuation strength (FS_5)), however, do not present major variations compared to the baseline case, see Figs. 4d and 4e, respectively. Lastly, the global psychoacoustic annoyance (PA) metric presents consistent reductions up to 20% in all the emission directions investigated. All in all, these results seem to indicate that the optimized propeller does indeed provide substantial reductions in noise annoyance for the same operational conditions at the thrust condition.

4. Conclusions

The present paper has demonstrated the potential of perception-influenced design for reducing propeller noise annoyance. A low-signature optimized propeller design was experimentally tested in an anechoic chamber, and its sound emissions were compared to a baseline propeller in terms of conventional and psychoacoustic noise metrics. The optimized propeller consistently provided lower noise values in all metrics considered while maintaining the desired thrust conditions. Future research will include dedicated listening experiments to confirm these claims.

Acknowledgments

This publication is part of the project *Listen to the future* (with project number 20247) of the research programme Veni 2022 (Domain Applied and Engineering Sciences) granted to Roberto Merino-Martinez which is (partly) financed by the Dutch Research Council (NWO).

REFERENCES

1. Burkard, R. and Hecox, K. The effect of broadband noise on the human brainstem auditory evoked response. I. Rate and intensity effects, *The Journal of the Acoustical Society of America*, **74** (4), 1204–1213, (1983).

2. Landström, U., Åkerlund, E., Kjellberg, A. and Tesarz, M. Exposure levels, tonal components, and noise annoyance in working environments, *Environment International*, **21** (3), 265–275, (1995).

3. Greenwood, E., Brentner, K. S., Rau, R. F. and Ted Gan, Z. F. Challenges and opportunities for low noise electric aircraft, *International Journal of Aeroacoustics*, **21** (5-7), 315–381, (2022).

4. Fastl, H. and Zwicker, E., *Psychoacoustics – Facts and models*, Springer Series in Information Sciences, Third edn., ISBN: 987–3–540–68888–4 (2007).

5. Osses, A., Greco, G. F. and Merino-Martinez, R. Considerations for the perceptual evaluation of steady-state and time-varying sounds using psychoacoustic metrics, 10^{th} *Convention of the European Acoustics Association (Forum Acusticum), September 11 – 15 2023, Torino, Italy*.

6. Greco, G. F., Merino-Martinez, R., Osses, A. and Langer, S. C. SQAT: a MATLAB-based toolbox for quantitative sound quality analysis, 52^{th} *International Congress and Exposition on Noise Control Engineering, August 20 – 23 2023, Chiba, Greater Tokyo, Japan*.

7. Kvurt, A., Ruf, D., Hertzman, O., Stalnov, O. and Ben-Gida, H. getPROP - A MATLAB suite for low-noise signature propeller design, analysis, and optimization, *AIAA SciTech Forum, 23-27 January, National Harbor, MD & Online*, (2023).

8. Selig, M. Low reynolds number airfoil design lecture notes, *VKI Lecture Series, November*, pp. 24–28, (2003).

9. Merino-Martinez, R., *Microphone arrays for imaging of aerospace noise sources*, Ph.D. thesis, Delft University of Technology, ISBN: 978–94–028–1301–2, (2018).

10. Greco, G. F. and Merino-Martinez, R. and Osses, A., (2023), *SQAT: a sound quality analysis toolbox for MATLAB (version v1.0)*. DOI: 10.5281/zenodo.7934710.